Collapse of homopolymer chains with two fixed terminals

Bin Xue, Jun Wang, and Wei Wang[a)]
National Solid State Microstructure Lab, Institute of Biophysics and Department of Physics, Nanjing University, Nanjing 210093, China

(Received 2 April 2003; accepted 11 July 2003)

We present molecular dynamics studies on the collapse of homopolymer model chains when two terminals are fixed over a selected distance. At low temperature, short chains show only β-hairpinlike conformations in their equilibrium; while the chain is long enough, helixlike conformations occur. A critical chain length serves as a boundary to distinguish the systems with different equilibrium behaviors and to separate three regimes of scaling behaviors between the mean square radius of gyration and the chain length. For short chains with a small end separation, namely, the end-to-end distance is below a specific value, the radius of gyration and asphericity index of the chain are independent of the end-to-end distance. When the end-to-end distance is larger than a specific distance, the radius of gyration and asphericity index grow linearly. For long chains, both the radius of gyration and asphericity index show multistage processes for different end-to-end separations. The Lindemann index and the asphericity index are combined together with the specific heat to describe the transitions of the chain's conformation following the variation of temperature.
 [DOI: 10.1063/1.1605732]

I. INTRODUCTION

Recently, the formation of various morphologies and conformations of homopolymers with specific constraints has been an interesting topic.[1–8] There are many types of constraints. The most common constraint is an infinite surface on which one end of the polymer chain is bound to form a grafted polymer chain or polymer brush when many chains are aligned.[2] A similar constraint is two parallel infinite surfaces. The chain between these two surfaces can be either fully flexible[4,6] or semiflexible. It corresponds to the flexible polymer melts[5] or the semiflexible melts[3] when many chains are involved. The single surface constraint can be further developed as a spherical pore.[9] Another kind of frequently used constraint is the restriction within polymer systems, such as the star-branched polymer,[7] which consists of many chains with one common end, and polymer chains can strongly interact with each other to form polymer melts. In addition, the star-branched polymer can also be confined between two parallel surfaces.[8] For some of the above-mentioned cases, the properties of scaling relations,[4,6,7] density profiles,[3–5] dynamic processes,[5,7,8] and thermodynamic behaviors[7] are well studied. The study on the dynamic behaviors of the formation of some specific patterns (or morphologies) and the conformational features of the homopolymer chains with different geometric constraints has both theoretical and practical importance,[7,10,11] for example, in the adsorption processes, the colloidal stability, and the surface polymerization. Moreover, the studies on the constrained homopolymer may provide us some physical implementations on proteins and DNA in biological environment.

In this paper we report a study on the conformational collapse and the relevant dynamic and thermodynamic behaviors of homopolymer chains of which two ends are fixed over a distance. This model can mimic the low-density cross-link, docking, and many other situations. Especially, in the thermal unfolding of proteins that have disulfide bonds, most hydrogen bonds are broken except the disulfide bonds due to their large strength of the chemical binding. Consequently, during the following refolding process, the residues linked by disulfide bonds could be treated as two fixed ends and the other parts of the polypeptide chain will fold under such a kind of restriction. In addition, even in the pure folding process, the disulfide bond could be formed before other non-sulfide bonds; this is also a starting point of our model. Therefore, in this work, we do not focus our interests on proteins or polypeptide chains that are heteropolymers,[12] but to a rather general case of flexible homopolymer chains. The distance between consecutive monomers and the potential function is chosen more appropriately for homopolymers and is similar to that in protein systems to some extent. Through the simulations on the collapse and folding, we expect that the dynamic and thermodynamic behaviors are different from the situation without the restriction on the ends since this kind of restriction greatly reduces the possible conformational space of the chains. The paper is arranged as follows: In Sec. II, we introduce the model and the simulation method. In Sec. III, we present and discuss the results. Then we provide a summary in the final section.

II. MODEL AND METHOD

The homopolymer is modeled as a chain composed of a number of monomers that are connected by bonds. Each monomer in the chain is treated as a bead with a certain radius. The radius of each bead provides the effect of excluded volume, which will be discussed later. The chain length is referred to as the number of the beads N. The total

a)Electronic address: wangwei@nju.edu.cn

potential of the chain system is a summation of the bond potential between consecutive beads and the van der Waals interaction among nonconsecutive beads as

$$U = U_{\text{bond}} + U_{\text{LJ}}. \tag{1}$$

The interaction of the bonds between the consecutive beads is modeled by a quadratic and quartic potential

$$U_{\text{bond}} = \sum_{j=1}^{N-1} k_1 (r_{j,j+1} - d_0)^2 + k_2 (r_{j,j+1} - d_0)^4, \tag{2}$$

where $r_{j,j+1}$ is the distance between two consecutive beads j and $j+1$ and d_0 is the equilibrium length of the bond and is set to be 3.8 Å. Here, the value of 3.8 Å corresponds to the length of the *trans* peptide bond[13] in proteins. The choice of this value for the potential of bond length validates some quantitative comparisons with protein systems. $k_1 = \varepsilon$ and $k_2 = 100\varepsilon$ are the interaction strengths with ε being the reduced energy unit.[14] The quadratic term characterizes the consecutive beads as a harmonic oscillator, while the quartic term acts as a ''soft clamp'' to restrict the beads within the distance not far away from the equilibrium position $r = d_0$. For the interaction between two nonconsecutive beads, a 12-6 Lennard-Jones (LJ) potential is used:[14–16]

$$U_{\text{LJ}} = \lambda\varepsilon \left[\left(\frac{\sigma_{ij}}{r_{ij}} \right)^{12} - 2 \left(\frac{\sigma_{ij}}{r_{ij}} \right)^{6} \right]. \tag{3}$$

Here λ is the interaction strength, r_{ij} is the distance between two nonconsecutive beads i and j, and σ_{ij} is the equilibrium distance between them. Due to the homogeneity of the chain and for the sake of simplicity, every σ_{ij} is set to be 6.5 Å. It is noted that the solvent effect is implicitly combined into the above potential, Eq. (3). The interaction strength λ can be adjusted to mimic different solvent conditions. Obviously, the polymer chains under consideration have good flexibility, and we do not restrict our simulation only to proteins. The potential does not include the local conformational constraints and the heterogeneity that exist in protein systems, the conformational constraints are usually represented by the bond-angle potential and the dihedral angle potential.[15]

The molecular dynamics (MD) method is used to simulate the collapse processes of the model chains by numerically solving the Newtonian equations of the beads on the chain through the leapfrog algorithm.[17] To keep the simulation in a canonical ensemble, the rotational and translational movements of the whole chain are scaled off at each step. The integration time step h in the simulation is set as $h = 0.005\tau$, where $\tau = a\sqrt{m/\varepsilon}$ is the characteristic time of the system with m the mass of the bead. (Actually, when these parameters are chosen as the characteristic quantities related to the realistic systems as $m = 3 \times 10^{-22}$ g, $\varepsilon = 1$ kcal/mol, and $a = 5$ Å, the characteristic time is about 3×10^{-12} s, and the integration time step is about 15 fs.[18]) Reduced units are used, namely $m = 1$, $\varepsilon = 1$, $a = 1$, $\tau = 1$. The time of simulations is measured with the number of the integration steps. Besides, we set $k_B = 1$, and hence the temperature $T = \varepsilon / k_B$ is also in reduced units. Since we are interested in the properties of polymers at a constant temperature, the Berendsen velocity scaling method is adopted to realize the canonical ensemble in our simulations.[19] The Berendsen coupling coefficient b is set as $b = 0.005$. Simulated annealing is used, i.e., the chain is first heated to a high temperature of $T = 2.0$ and equilibrated for 5×10^4 time steps, and then the temperature is slowly cooled down by a coefficient of 0.9 until reaching the desired temperature. At each new temperature the chain is relaxed for 5×10^4 time steps. After reaching to the final desired temperature, the simulation ends at 5×10^7 time steps.

The initial conformation of the chain is set to be a necklacelike ring without any contacts, and the initial velocities are set to satisfy Maxwell's distribution at the given temperature. In order to calculate the ensemble average for the system, we perform up to 20 runs of simulated annealing MD simulations under different initial velocities for each chain length and for each temperature. The data are sampled every 4×10^3 time steps after the system reaches the equilibrium.

The conformational properties studied in this paper include the radius of gyration R_g, the helicity order parameter H,[20] the asphericity index A, and the Lindemann index L.[21] The helicity order parameter H is defined as

$$H = \sum_i (\mathbf{r}_{i,i+1} + \mathbf{r}_{i+1,i+2} + \mathbf{r}_{i+2,i+3})^2 \times \text{sgn}[(\mathbf{r}_{i,i+1} \mathbf{r}_{i+1,i+2}) \cdot \mathbf{r}_{i+2,i+3}], \tag{4}$$

where $\mathbf{r}_{i,i+1}$ is the bond vector between the ith and the $(i+1)$th beads and sgn$[\cdots]$ means to take the sign of the formula in the bracket. This definition is slightly different from that in Ref. 20, where, H does not have a summation over all the beads and is actually a measure of chirality for the α helix. Thus in our model, H is a parameter of helicity of any form of helices and can be applied to demonstrate the position of helices in the chains. The asphericity index is defined as

$$A = \frac{(L_1^2 - L_2^2)^2 + (L_2^2 - L_3^2)^2 + (L_3^2 - L_1^2)^2}{2R_g^4}, \tag{5}$$

in which L_1^2, L_2^2, and L_3^2 are the momenta of inertia in three main axes. For the sake of simplicity, in the following discussion we suppose $L_1^2 \leqslant L_2^2 \leqslant L_3^2$. The value of A is between [0,1]. $A = 0$ is caused by $L_1^2 = L_2^2 = L_3^2$ and is referred to as a perfect spherical globe, while $A = 1$ is due to $L_1^2 = L_2^2 = 0$ or other similar cases and represents a rod. $A = 0.25$ is derived from $L_1^2 = 0$, $L_2^2 = L_3^2$, and depicts a circle. Usually in practice, for a spherical conformation, the value of A is less than 0.1; for a rodlike conformation, the value of A is larger than 0.6; for a toroid the value of A is between 0.15 and 0.25. The Lindemann index actually describes the fluctuation of interbead distances and is defined as

$$L = \frac{2}{N(N-1)} \sum_{i<j} \frac{\sqrt{\langle r_{ij}^2 \rangle - \langle r_{ij} \rangle^2}}{\langle r_{ij} \rangle}. \tag{6}$$

In a normal solid-state system one has $L < 0.1$. Hence the change in Lindemann index could be used to measure the phase transition from liquid to solid state.

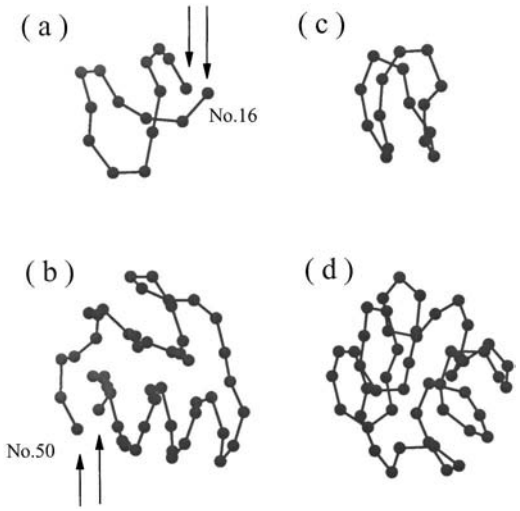

FIG. 1. The equilibrium conformations at $t=4\times10^7$, $T=0.1$, and $\lambda=1$. (a) and (b) are for two chains with $r_d=6.5$ and different chain length N. The arrows point out the fixed beads, the two labels "No. 16" and "No. 50" indicate the 16th and the 50th monomer of each chain, respectively. (a) $N=16$; (b) $N=50$. (c) and (d) are for ring homopolymers with $N=16$ and $N=50$, respectively.

To present the thermodynamic properties of the systems, we calculate the heat capacity over a series of temperatures. The heat capacity is calculated by

$$C_V(T)=\frac{\langle E_T^2\rangle-\langle E_T\rangle^2}{T^2}, \tag{7}$$

where E_T is the total energy at temperature T, and $\langle\,\rangle$ over E_T^2 and E_T denotes the average obtained from samples on one trajectory. Then the ensemble average of $C_V(T)$ is obtained over a number of trajectories.

III. RESULTS AND DISCUSSION

We perform the simulated annealing MD studies on homopolymer chains of different lengths. The simulations are carried out at a series of temperatures, with various end-to-end distances r_d and under several interaction strengths λ. We present the conformational, dynamic, and thermodynamic properties as follows.

A. Conformational properties

Figure 1 shows the conformational difference between two homopolymer chains with different chain lengths. The two homopolymer chains have the same end-to-end distances $r_d=6.5$ Å, and are equilibrated at the same temperature $T=0.1$, but their lengths are $N=16$ and $N=50$, respectively, as in Figs. 1(a) and 1(b). Apparently, the short chain with $N=16$ does not have the helixlike conformation but a β-hairpinlike pattern. For the longer chain with $N=50$, besides the β-hairpinlike pattern, the helixlike conformation can be observed too. Especially in one-half of the chain, there is a regular conformation of the helix. Since the model here is very close to the ring polymer, a comparison with ring polymers would be interesting. We present the equilibrium conformations of ring homopolymer chains with lengths $N=16$ and $N=50$ in Figs. 1(c) and 1(d), respectively. The results show that for ring homopolymers, the conformational properties are almost the same as those of homopolymers with two fixed ends. We expect that the other properties of the chain with two fixed ends will be also very similar to that of the ring polymer when the end-to-end distance does not deviate much from the bond length. When the end-to-end distance is much longer than the bond length, these two kinds of polymers with the same length are very different. The detailed results will be presented elsewhere.

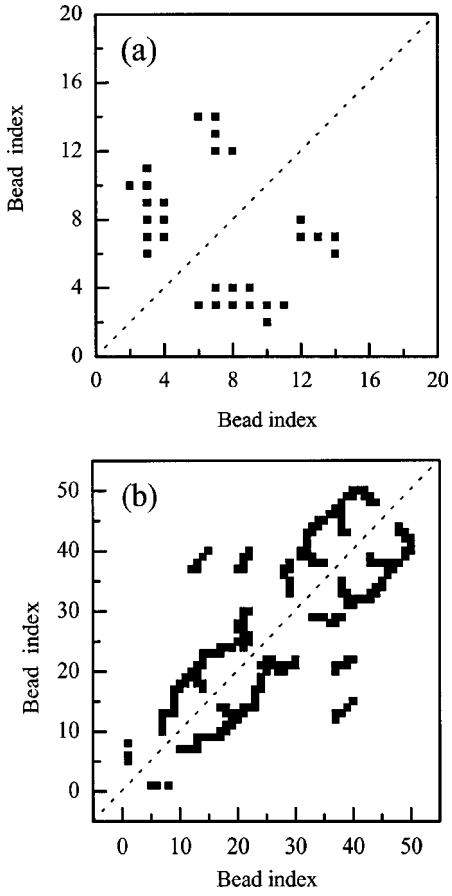

FIG. 2. Contact maps corresponding to Figs. 1(a) and 1(b). (a) $N=16$, the dots parallel to the axes indicate the loop conformation, the dots parallel to the descending diagonal represent antiparallel β-like conformation; (b) $N=50$, the equal-distance dots parallel to the ascending diagonal mean helix-like conformation.

To further illustrate the conformational characteristics of the chains in Figs. 1(a) and 1(b), we present the contact maps of snapshots in Figs. 2(a) and 2(b), respectively. The snapshots are extracted at $t=4\times10^7$ at which the chain systems have reached their equilibrium states. From Fig. 2(a), we can see that the chain with $N=16$ only has the β-hairpinlike conformation near the ninth and tenth beads, and the dots parallel to the axes indicate the looplike conformation. In many cases, the loop conformation is beneficial for the packing effect. Figure 2(b) shows the contact map for the case of $N=50$. The chain has helixlike conformations near the 20th and 40th beads.

In Fig. 3, we plot the helicity order parameter H for the chain with $N=50$ to show the presence and evolution of helices. Figure 3(a) shows the change of H along the chain at the time of $t=4\times10^7$. It is clear that in the place where

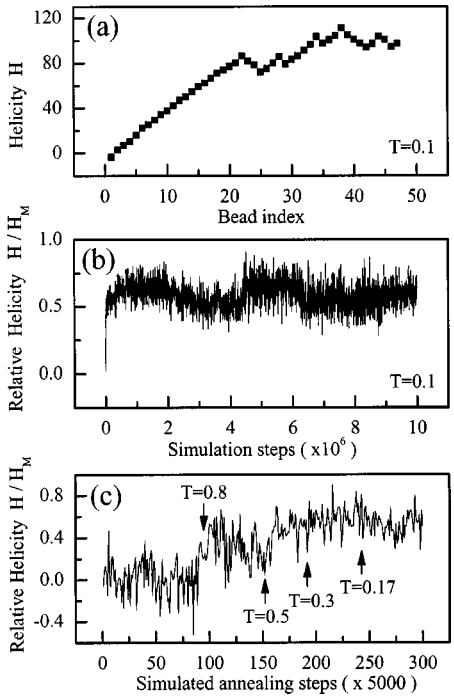

FIG. 3. For a chain with $N=50$. (a) The value of helicity H along with the chain at the snapshot of $t=4\times10^7$. (b) The relative helicity H/H_M as a function of simulation time. The simulation temperature is 0.1. (c) The change of relative helicity H/H_M during the annealing process. The temperature varies from 2.0 to 0.1 by a cooling coefficient of 0.9, and the relaxation time in each new temperature is 5×10^7.

$N<22$, H increases linearly with N; hence in this range, the chain forms a helix as previously shown in Figs. 1(b) and 2(b). Also the 30th to 38th beads form a helixlike winding as well. However, in general, the value of H behind the 22nd bead does not have linear behavior; hence there is no regular helical conformation. As a result, almost half of the chain takes the helical conformation. It is worth noting here that in this model there are eight beads in one winding of spiral, and the value of H increases by about 20. If all the 50 beads in the chain are involved in the formation of this type of helix, $H=188$, which is defined as H_M, i.e., the maximum value in this situation. Therefore, for any kinds of conformation, the ratio H/H_M is the composition of the helix in that conformation.

In Fig. 3(b) we give the time evolution of H/H_M at $T=0.1$ for the chain with $N=50$. The trajectory used here is truncated at $t=10^7$ time steps. It is shown that about more than half of the chain is in the helical conformation most of the time. These data are slightly higher than those we give in Fig. 3(a). The reason is that when we calculate H, even the beads not forming a regular helix can contribute to the value. As shown in Fig. 3(a), the 30th to 38th beads will contribute to H, but they do not form a helix. Also in Fig. 3(b) we find that due to the existence of the end constraints, the chain forms a helix very quickly and then fluctuates around the equilibrium. This is probably caused by the greatly reduced conformational space.

Figure 3(c) shows the change of H/H_M during the annealing process. The annealing process is described in Sec. II. In the figure, the temperature at the left side is higher than that at the right side. We can see from this figure that when the temperature is higher than $T=0.8$, $H/H_M\sim0$; hence the chain is like a random coil. Further decreasing the temperature, the average value of H/H_M is bigger than zero, that is, there are helical patterns in the chain. When $T<0.3$, $H/H_M\sim0.6$, which indicates half of the chain have helical conformation. This is in accordance with the result from Fig. 3(b). These two key temperatures of $T=0.3$ and $T=0.8$ act as the boundaries of large changes of conformations and will be analyzed further in Sec. III C.

The physical reasons for the existence of different conformations can be understood as follows: Under the force field considered in this work and at the temperature of $T=0.1$, forming one winding of spiral needs around 8 or 9 beads. This can be seen from Fig. 2(b) clearly. Forming the prototype of a helix needs at least two windings of spirals. Taking into consideration the connection to another fixed terminal, the minimum number of monomers for observing a helixlike conformation should be at least 20. The actual simulation results also show that a chain with length $N=20$ has helixlike conformation, but a shorter chain with length $N=16$ does not have helical conformation (figure not shown). At higher temperatures, for example, $T=0.7$, the chain with $N=20$ loses the helical shape and degenerates to a random coil due to the ''unfolding'' effect. It is natural to think that if we decrease the number of beads needed for forming one winding of spiral, then the chain length for observing a helixlike conformation should decrease and *vice versa*. This can be easily achieved by changing the interaction strength λ. Increasing the value of λ means to increase the attraction among the beads and hence to decrease the number of beads needed for the formation of one winding of spiral. Put another way, decreasing the value of λ will increase the number of beads for forming one winding of spiral. Thus in the case of $\lambda=2$, the chain length necessary for observing the helixlike conformation will be shorter than that in the case of $\lambda=1$.

Our simulation at $\lambda=2$ and $T=0.1$ for a chain with $N=16$ shows that the chain has a helixlike conformation with six beads forming one winding of spiral. Further detailed simulations show that under this circumstance the minimum chain length for observing a helixlike conformation is $N=16$. We also decrease the value of λ from 1 to 0.5, and find that the chain with $N=20$ loses its helixlike conformation. As a result, chains with different lengths have different conformations. The critical chain length for having a helixlike conformation under the conditions of $T=0.1$ and $\lambda=1$ is $N=20$. Increasing the interaction strength λ may reduce this critical length. It is noted that such a critical length exists only when the temperature is not too high since at high temperature the ordered conformation will be modified to random coil.

The above results imply that the chain length N may play an important role in the formation of the conformations, especially at low temperatures. Hence we study the scaling relation between the mean square radius of gyration R_g^2 and the chain length N. Figures 4(a) and 4(b) show the scaling relations for $\lambda=1$ and $\lambda=2$, respectively. In both figures, the chain length varies from $N=10$ to $N=50$ (the case of

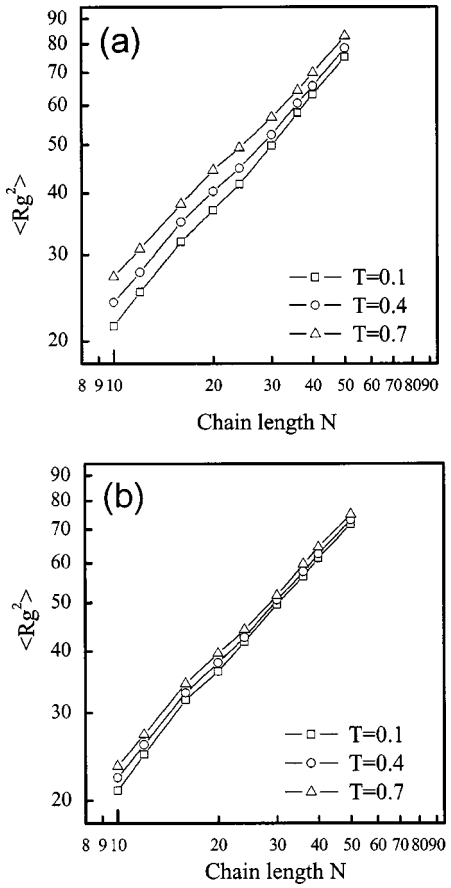

FIG. 4. The scaling relations between the mean square radius of gyration R_g^2 and the chain length N at temperatures $T=0.1$, 0.4, and 0.7, with the end-to-end distance $r_d=6.5$ and the interaction strength (a) $\lambda=1$; (b) $\lambda=2$.

$N>50$ will be discussed elsewhere), and the simulation temperatures are $T=0.1$, $T=0.4$, and $T=0.7$. In Fig. 4(a), it is clear that all the scalings show three different regimes. These three regimes can be simply distinguished as the short-chain regime with $N<16$ or so and the long-chain regime with about $N>24$, and there is a crossover between them. Under the short-chain regime, the scaling is $\langle R_g^2\rangle \sim N^{\nu_S}$ with $\nu_S \sim 0.84$, while in the long-chain regime, the scaling is $\langle R_g^2\rangle \sim N^{\nu_L}$ with $\nu_L \sim 0.81$. It is noted that the values of these two scaling exponents are more or less the same. It is also worth noting that the scaling relation for the self-avoiding walk (SAW) chain is $\langle R_g^2\rangle \sim N^{\nu}$, where $\nu \sim \frac{2}{3}$.[22,23] As a comparison, at the crossover range, i.e., the medium-chain size, we have a scaling exponent $\nu \sim 0.66$, which is quite similar to that of the SAW chain. However, at both the short-chain and the long-chain limits, the scaling exponents ν_S and ν_L are greater than that of the SAW chain.

The variance in the exponents shows different increasing rates of the volume of the chain. Under the circumstances with a fixed end-to-end distance, at the crossover range, the two fixed terminals provide more conformational space for the chain, leading to a slowing down of the increasing of volume. Also from Fig. 4(a), we can see that the chain length corresponding to the crossover region increases as the temperature increases. For example, in the case of $T=0.1$, the crossover starts at about $N=16$, at $T=0.4$ the crossover begins at around $N=18$, and at $T=0.7$ it is at $N=20$. Correspondingly, the crossovers finish at $N=24$, 26, and 30. The physical reason for this drifting phenomenon is that at higher temperatures, the volume of the chain is larger than that a lower temperatures. Thus longer chains can arrange themselves within the same volume as at the lower temperatures; hence the increase of R_g slows down.

From the above discussions, we can see that how to define the crossover is of great interest. In Fig. 4(b) we show the scaling relations at $r_d=6.5$ and $\lambda=2$ to see the definition of crossover. The first notable change compared with Fig. 4(a) is that the distances between lines at various temperatures are reduced. This is solely the effect of the increase in the interaction strength. The scaling formula for Fig. 4(b) is $\langle R_g^2\rangle = cN^{\nu}$, where c denotes a small distance between lines and small increasing ratio for R_g^2. The second difference compared with Fig. 4(a) is that there is almost no drifting in the beginning length of the crossover at different temperatures. That is, all the starting and ending chain lengths corresponding to the crossovers are $N=16$ and $N=24$, respectively. Previously, we explained the drifting by the extra conformational space. Here, due to the strong interaction among the monomers, there is hardly any extra conformational space for longer chains at relatively higher temperatures. Thus, the drifting disappears. At the same time, the scaling exponent at short-chain limits is $\nu_S=0.89$, and at long-chain limits $\nu_L=0.73$. Compared with Fig. 4(a), the value of the scaling exponent under short-chain regime increases; but decreases under the long-chain regime.

In Ref. 24, the authors found that the scaling exponent for ring polymers is 0.84, which is similar to the situation for short-chain length and weak interaction in our study, but different from others. The main reason is that the end-to-end distance of the polymer with two fixed ends does not equal the bond length, but in a ring polymer all the distances are the same. Thus, the relations shown in Fig. 4(b) reflect the influence of the end-to-end distance on the system and make the chains of polymers with two fixed ends different from the ring polymers.

Actually, the chain length in the crossover range is independent of temperature T in the case of strong interactions, e.g., $\lambda=2$. When interaction strength is relatively weak, e.g., $\lambda=1$, the chain length in the crossover range becomes slightly longer at higher temperatures. In the case of strong interactions, the starting chain length for observing the crossover is the critical chain length beyond which the chain has helixlike conformation. The reason is that the chain is highly compact under the influence of strong interaction λ. For those chains with length longer than $N=16$, the compact construction can be changed from solely β-hairpinlike into both β-hairpinlike and helixlike. Hence the scaling relation is changed at this point. Put another way, under the weak interaction, chains are not so compact and their conformations can be adjusted slightly. Thus, the scaling relations are distorted to some extent.

The scaling of R_g on the chain length N shows a power law. However, it is interesting to know whether the increment of R_g has a preferential direction. In other words, do the momenta of inertia in the three main axes grow with the

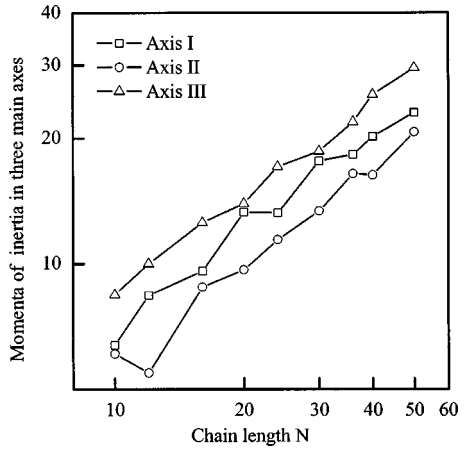

FIG. 5. Scaling relations between three main axes of momenta of inertia and the chain length N. The relevant parameters are $T=0.1$, $r_d=6.5$, and $\lambda=1$.

chain length simultaneously or not? We clarify this by illustrating the scaling relations between momenta of inertia and the chain length in the three main axes as shown in Fig. 5. From Fig. 5, it is clearly shown that although the accretions in the three main axes almost show the same trend, the moment of the third one (the direction along the two fixed ends) is larger than the other two. This really indicates an anisotropic growth or anisotropic change of the conformation.

To show the influence of end-to-end distance on the formation of the chains' conformations, we plot the radius of gyration R_g and the asphericity A for the equilibrium state against the end-to-end distance in Fig. 6. Here the radius of gyration R_g and the asphericity A indicate the general volume and rough shape of the chain systems. The end-to-end distance is given in reduced units which is the ratio of the actual distance to the chain length. From Fig. 6(a), it is seen that R_g and A are highly correlated and the correlation coefficient is around 0.97 at each temperature. This means that the increase of R_g is caused by weakening the effect of collapse or compaction of the chain systems. Figure 6(a) gives the results at two different temperatures for a chain with length $N=16$. Obviously, at $r_d/L=0.25$ there are sharp increments in both R_g and A. Clearly, $r_d/L=0.25$ is a critical value. When the end-to-end distance is less than this value, the values of R_g and A are kept almost unchanged. This means that the volume and the shape of the chain are unchanged and are independent of the increasing of the end-to-end distance. However, when $r_d/L>0.25$, both R_g and A increase linearly as the end-to-end distance increases. Hence, there are conformational transitions from globularlike to toroidlike, then to ellipsoidlike, and finally to a rodlike.

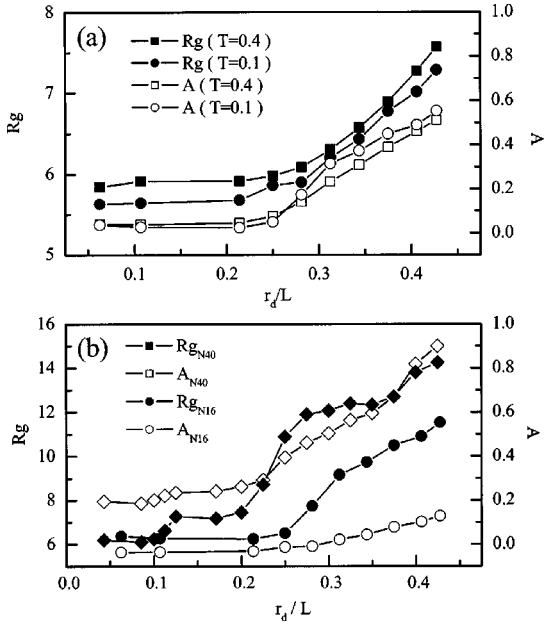

FIG. 6. Conformational changes at different end-to-end distances. (a) Radius of gyration R_g and asphericity index A as functions of reduced end-to-end distance for $N=16$ chain at two temperatures of $T=0.1$ and 0.4. The reduced end-to-end distance is defined as the ratio of actual end-to-end distance r_d to real the chain length $L=Nd_0$. (b) Changes of R_g and A with r_d/L at $T=0.1$ for two chains with $N=16$ and $N=40$, accordingly.

Figure 6(b) shows a comparison between results of two chains with $N=40$ and $N=16$ at $T=0.1$. From Fig. 6(b) one can see that the influence of the end-to-end distance on the conformation of the chain becomes complicated as the chain length increases. The main difference between the two cases is that there are additionally two plateaus for the chain with $N=40$. When the reduced end-to-end distance r_d/L is less than 0.1, both R_g and A are kept at $R_g\sim 8$ Å and $A<0.02$ when increasing r_d/L. Such a value of the asphericity index A indicates that the chain takes a spherical morphology. When r_d/L increases to 0.125, the values of R_g and A increase linearly to 8.4 and 0.12, respectively. The simultaneous increasing of these two quantities shows a picture that the volume increment of the chain is caused by the shape distortion. However, the resultant morphology is still spherical-like. Further increasing r_d/L to 0.2, both R_g and A show the second plateau where R_g and A do not change with increasing value of r_d/L. Then in the range of $0.275>r_d/L>0.2$, the value of R_g increases from 8.6 to 10.6, and the value of A increases from 0.15 to 0.6. The conformation changes from spherical-like to toroidlike and then to ellipsoidlike rapidly. In the following range up to $r_d/L=0.375$, A almost keeps a constant of 0.6 and the chain keeps its morphology as an ellipsoid. However, the value of R_g increases to 12.7. This is the only region where R_g and A do not keep the same pace. Also in this range the asphericity index has the third plateau, and the radius of gyration continues to rise. Finally, when $r_d/L>0.375$, both R_g and A increase again in a same way. The value of $A\sim 1$ means a rodlike conformation. Thus, as a result of the comparison between two chains with different lengths, the major discrepancies are the multiple stages and the appearance of the plateaus. For a short chain, the conformation only undergoes a single transition from one type to another, while for a long chain, the conformation undergoes multistep transitions. This is clearly due to the increased conformational entropy of the long chain, which leads to a more complicated dynamics.

B. Dynamic process

Here, we present the evolutions of total energy E and radius of gyration R_g along with the simulation time as

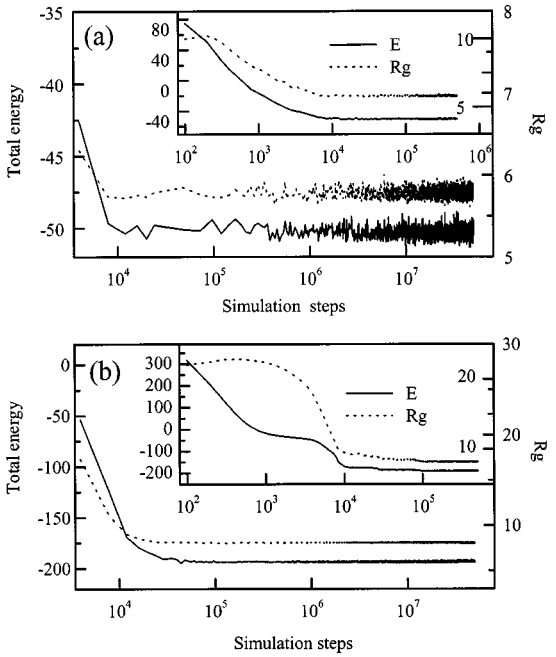

FIG. 7. Time evolutions of total energy and radius of gyration at $r_d=6.5$ and $\lambda=1$. The data are sampled every 4×10^3 time steps from trajectories of 5×10^7 time steps. The insets are extracted with small time intervals of $\delta t=100$ from the trajectories above and truncated at 5×10^5. The solid and the dotted lines indicate the total energy E and the radius of gyration R_g, respectively. (a) $N=16$; (b) $N=40$.

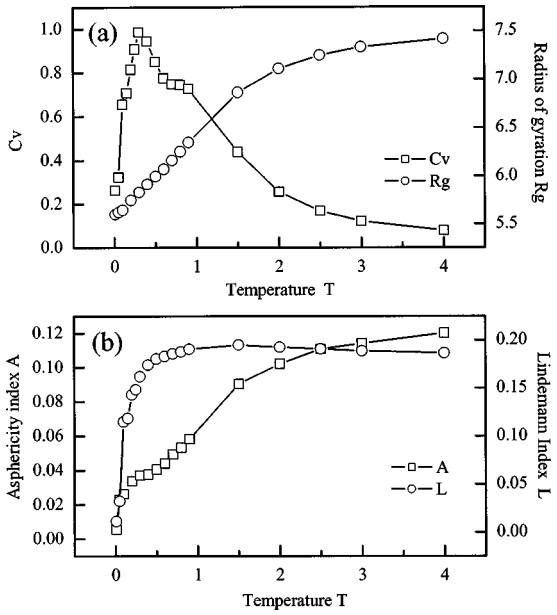

FIG. 8. Thermodynamic properties for chain with $N=16$ with $r_d=6.5$ and $\lambda=1$. (a) Specific heat C_V and radius of gyration R_g; (b) Lindemann index L and asphericity index A.

shown in Fig. 7. Figures 7(a) and 7(b) are for $N=16$ and $N=40$, respectively. Each plot in the main graph shows the data extracted every 4×10^3 time steps from a trajectory of 5×10^7 time steps, and the insets are the data extracted every 100 time steps from the trajectories above and truncated at 5×10^5 time steps. The general trends for both short and long chains are very similar, i.e., the total energy E and radius of gyration R_g decrease very quickly and then vibrate around their equilibrium values. For the chain with $N=16$, E is -50 and R_g is 5.8 at the equilibrium with the standard deviation of $\delta^2E=0.35$ and $\delta^2R_g=0.06$, respectively. For $N=40$, $E\sim-194$ and $R_g\sim8.1$ at the equilibrium with a standard deviation of $\delta^2E=1.47$ and $\delta^2R_g=0.09$, accordingly. We can also see that the times at which the total energy and radius of gyration reach their equilibrium values coincide with each other very well.

In the insets, the time evolutions of E and R_g are different for short and long chains. These are the short time pictures of the dynamic processes, which may strongly depend on the initial conditions. For the short chain with $N=16$, both E and R_g decrease smoothly while reaching the equilibrium. For the long chain with $N=40$, within the first 700 time steps, the radius of gyration keeps its value of $R_g\sim22$ while total energy decreases from $E\sim320$ to $E\sim6$; then from $t=700$ to $t=4\times10^3$, the total energy and the radius of gyration decrease slowly to $E\sim-50$ and $R_g\sim17$, respectively. In the following simulation to $t=10^4$, the total energy and the radius of gyration drop quickly to $E\sim-170$ and $R_g\sim9.5$, which are close to the above-mentioned equilibrium values. The special evolutions of E and R_g in the short time period are caused by the initial necklacelike conformation. At the first few steps, the chain changes from two-dimensional conformation to three-dimensional conformation. The energy will decrease due to the increased interaction, but the radius of gyration can keep almost unchanged.

C. Transitions of conformations

Now let us study the phase behaviors. Figures 8(a) and 8(b) show the heat capacity C_V, the radius of gyration R_g, the Lindemann index L, and the asphericity index A as functions of temperature T. The heat capacity shows a sharp peak around $T=0.3$ and a shoulder near $T=0.8$. These imply two transitions between different conformation ensembles. From Figs. 8(a) and 8(b), at the high-temperature limits, C_V approaches zero, while R_g increases to a saturated value of 8. This is an indication that the chain is in a vaporlike phase, and the conformation is loose. As the temperature decreases, R_g shows a slow decrease until the temperature reaches a value slightly higher than $T=1$, and in this stage the volume of the chain shrinks gradually. Further decreasing the temperature from around $T=1$ to $T\sim0$, R_g decreases linearly and quickly. It is clear that due to the weakening of the monomers' thermal movement, the possible repulsion caused by the thermal movement can be decreased steadily and the attraction among the monomers is enhanced. Thus the chain can collapse to more compact conformation.

The Lindemann index L also shows a saturated value of 0.19 at the high temperature limits. From $T=1.5$ to 0.6, the values of L decrease slowly from 0.19 to 0.18. This slow change may correspond to the shoulder shown in the C_V curve. Since the Lindemann index is the measurement for the position fluctuation of the monomers, decreasing of L means to improve the order of the system. We can see that from $T=0.6$ to $T\sim0$, the values of L change greatly from 0.18 to 0.01. This really relates to the peak in the C_V curve. It is

known that usually the system is in a solid state when the Lindemann index is less than 0.10. Therefore, it is reasonable to believe that in this temperature range there has been a phase transition leading the chain to a solid phase, i.e., the compact conformation. The sharp peak in C_V indicates such a transition.

In Fig. 3(c) we show that when the temperature is decreased to $T\sim 0.8$, there is a conformational change from the random coil to a partly helical one; at $T\sim 0.3$, the number of helices increases greatly and indicates a more ordered conformation. These two temperatures are just the same as in the above discussions. In addition, as shown in Fig. 8(b), above $T=2$, the value of A is greater than 0.1, implying that the chain takes the conformation other than the spherical. This is the influence of the fixed terminals. As the temperature decreases, the value of A decreases accordingly. The interesting thing is that within the temperature range of $0.5>T>0.15$, the change of A slows down. According to the definition of A, this possibly means that the three main axes of inertia keep unchanged. By taking into consideration of Fig. 8(a), the value of R_g does decrease within this temperature range too. Thus, we may ascertain that the chain simply shrinks when the temperature is decreasing through this range. This may also be the evidence that the transition around $T=0.3$ leads the chain into a solid state, or a more stable and compact conformation.

IV. SUMMARY

We study the various properties of homopolymer chains by the canonical molecular dynamics method. In the model studied in this paper, the two terminals are placed on two static points. Thus, not only the distance between the two ends is constant, but also the position vectors of the two ends are constants. Hence, the chain system rotates around the fixed axis that links the two ends. Then during the simulations, the translational and rotational movement of the chain are removed at each step. This situation resembles the adsorption phenomenon. In the cases of the thermal unfolding and refolding of proteins that have disulfide bonds, since the studied system is usually only a small part of the very long chain, the amino acid residues forming the disulfide bond can be considered as fixed in space. However, another model in which the rotation is around the mass center could also be possible. In such a model the distance between two ends is a constant, but the two ends can move in the space. In this case, the rotational movement around the mass center shall be removed.

The conformational differences between chains of different lengths are analyzed when their two ends are fixed. The short chains only show the β-hairpinlike conformations, whereas the longer chains have both the β-hairpinlike and helixlike conformations at low temperatures. The critical chain length is determined by the number of monomers needed for forming the prototype of the helix by composing two windings. If the end-to-end distance increases, more monomers will be needed to form the helix. However, the effect is less prominent. Enhancing the interaction strength can reduce the number of monomers needed for forming one winding, and thus reduce the value of critical length. Raising the temperature brings about the ''unfolding'' phenomenon and diminishes the conformational differences between long and short chains. It is interesting to note that if the two ends of the homopolymer chains are free, within the range of the discussed chain lengths, the chains always have helixlike conformations after reaching equilibrium at low temperature.[14]

The scaling relations between the mean square radius of gyration and chain length are also studied at different temperatures and interaction strengths. Three scaling regimes, namely, the long-chain regime, the short-chain regime, and the crossover between them, are found. The behaviors of chains in the crossover range resemble those of the SAW homopolymer chains. The short- and long-chain length regimes show remarkable differences compared to the SAW chains. Under a strong interaction, the critical chain lengths corresponding to the crossover are independent of the temperature, whereas under a relatively weak interaction, the critical chain lengths corresponding to the crossover drift slightly to the long-chain side as the temperature increases. The combination of the analyses on the conformations and the scaling relations indicates that the internal structure of the chain plays an important role in the conformational properties of the system.[25] The internal structure of the chain is affected by the interaction strength, the end-to-end distance, and the chain length as well. Through the studies on the momenta of inertia in three main axes, we find that for a system with long-chain length, the shapes of the compact conformations of the chains are anisotropic.

The end-to-end distance affects the conformation of the chain greatly. For short chains, when the ratio of chain length to the end-to-end distance is small, the radius of gyration and the asphericity index remain unchanged when the end-to-end distance is increased. While the ratio is greater than a specific value, the radius of gyration and the asphericity index increase linearly with increasing end-to-end distance. For long chains, the asphericity index and the radius of gyration show multiple-stage behaviors and have many plateaus.

The phase transition behaviors of the system are studied as well. The specific heat, the radius of gyration, the asphericity index, and the Lindemann index are combined to illustrate two transitions in the system. The specific heat shows a peak and a shoulder. The peak corresponds to the collapse of conformation, which indicates a transition to compact structure. This is similar to the solid–liquid transition as characterized by some other structural properties.

ACKNOWLEDGMENTS

This work was supported by the National Natural Science Foundation of China (Grant Nos. 90103031, 10074030, and 10021001), and the Nonlinear Project (973) of the NSM.

[1] P. G. de Gennes, *Scaling Concepts in Polymer Physics* (Cornell University Press, Ithaca, New York, 1979).
[2] S. T. Milner, Science **251**, 905 (1991).
[3] A. Yethiraj, J. Chem. Phys. **101**, 2489 (1994).
[4] A. Milchev and K. Binder, Eur. Phys. J. B **3**, 477 (1998).
[5] T. Aoyagi, J. Takimoto, and M. Doi, J. Chem. Phys. **115**, 552 (2001).
[6] J. H. Vliet and G. ten Brinke, J. Chem. Phys. **93**, 1436 (1990).
[7] P. Romiszowski and A. Sikorski, J. Chem. Phys. **109**, 2912 (1998).

[8] P. Romiszowski and A. Sikorski, J. Chem. Phys. **116**, 1731 (2002).
[9] D. K. Klimov, D. Newfield, and D. Thirumalai, Proc. Natl. Acad. Sci. U.S.A. **99**, 8019 (2002).
[10] K. De'Bell and T. Lookman, Rev. Mod. Phys. **65**, 87 (1993).
[11] C. E. Woodward, J. Chem. Phys. **97**, 4525 (1992).
[12] J. Wang and W. Wang, Phys. Rev. E **61**, 6981 (2000).
[13] A. Liwo, S. Oldziej, M. R. Pincus, R. J. Wawak, S. Rackovsky, and H. A. Scheraga, J. Comput. Chem. **18**, 849 (1997).
[14] C. Clementi, A. Maritan, and J. R. Banavar, Phys. Rev. Lett. **81**, 3287 (1998).
[15] S. Takada, Z. Luthey-Schulten, and P. G. Wolynes, J. Chem. Phys. **110**, 11616 (1999).
[16] H. Noguchi and K. Yoshikawa, J. Chem. Phys. **113**, 854 (2000).
[17] M. P. Allen and D. J. Tildesley, *Computer Simulation of Liquids* (Clarendon, Oxford, 1989).
[18] T. Veitshans, D. Klimov, and D. Thirumalai, Folding Des. **2**, 1 (1997).
[19] H. J. C. Berendsen, J. P. M. Postma, W. F. van Gunstern, A. Dinola, and J. R. Haak, J. Comput. Phys. **81**, 3684 (1984).
[20] P. Romiszowski and A. Sikorski, Biopolymers **54**, 262 (2000).
[21] H. Noguchi and K. Yoshikawa, J. Chem. Phys. **109**, 5070 (1998).
[22] K. Kremer, A. Baumgartner, and K. Binder, J. Phys. A **15**, 2879 (1981).
[23] G. Tanaka and W. L. Mattice, Macromol. Theory Simul. **5**, 499 (1996).
[24] S. Brown and G. Szamel, J. Chem. Phys. **109**, 6184 (1998).
[25] K. Fan, J. Wang, and W. Wang, Phys. Rev. E **64**, 041907 (2001).